Hg–Xe Exciplex Formation in Mixed Xe/Ar Matrices: A Molecular Dynamics and Luminescence Study.

ARTICLE *in* THE JOURNAL OF PHYSICAL CHEMISTRY A · SEPTEMBER 2014

Impact Factor: 2.69 · DOI: 10.1021/jp5065038 · Source: PubMed

5 AUTHORS, INCLUDING:

Rolando Rafael Lozada García

Université Paris 13 Nord

7 PUBLICATIONS **21** CITATIONS

SEE PROFILE

Germán Rojas-Lorenzo

Instituto Superior de Tecnologías y Ciencias A…

32 PUBLICATIONS **273** CITATIONS

SEE PROFILE

Claudine Crépin

French National Centre for Scientific Research

84 PUBLICATIONS **599** CITATIONS

SEE PROFILE

Maryanne caroline Ryan

National University of Ireland, Maynooth

9 PUBLICATIONS **20** CITATIONS

SEE PROFILE

THE JOURNAL OF PHYSICAL CHEMISTRY A

Article

pubs.acs.org/JPCA

Hg−Xe Exciplex Formation in Mixed Xe/Ar Matrices: Molecular Dynamics and Luminescence Study

Rolando Lozada-García,[†] Germán Rojas-Lorenzo,[†] Claudine Crépin,*[,‡] Maryanne Ryan,[§] and John G. McCaffrey[§]

[†]Departamento de Física General, Matemática y Computación, Instituto Superior de Tecnologías y Ciencias Aplicadas, La Habana, Cuba

[‡]Institut des Sciences Moléculaires d'Orsay (ISMO)- UMR 8214, CNRS-Université Paris-Sud, Bâtiment 210 Université Paris-Sud, F-91405 Orsay, France

[§]Department of Chemistry, National University of Ireland-Maynooth, Maynooth, Co., Kildare, Ireland

Supporting Information

ABSTRACT: Luminescence of Hg($^3P_1$) atoms trapped in mixed Ar/Xe matrices containing a small amount of Xe is reported. Broad emission bands, strongly red-shifted from absorption are recorded which are assigned to strong complexes formed between the excited mercury Hg* and xenon atoms. Molecular dynamics calculations are performed on simulated Xe/Ar samples doped with Hg to follow the behavior of Hg* in the mixed rare gas matrices leading to exciplex formation. The role of Xe atoms in the first solvation shell (SS_1) around Hg was investigated in detail, revealing the formation of two kinds of triatomic exciplexes; namely, Xe−Hg*−Xe and Ar−Hg*−Xe. The first species exists only when two xenon atoms are present in SS_1 with specific geometries allowing the formation of a linear or quasi-linear exciplex. In the other geometries, or in the presence of only one Xe in SS_1, a linear Ar−Hg*−Xe exciplex is formed. The two kinds of exciplexes have different emission bands, the most red-shifted being that involving two Xe atoms, whose emission is very close to that observed in pure Xe matrices. Simulations give a direct access to the analysis of the experimental absorption, emission, and excitation spectra, together with the dynamics of exciplexes formation.

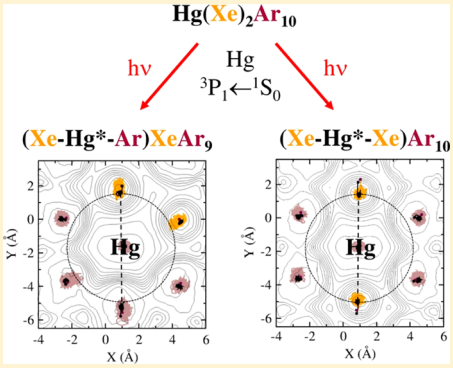

I. INTRODUCTION

The spectroscopy of mercury isolated in low-temperature solids has been the subject of a number of studies in the past decades, and in fact, the 6p $^3P_1 \leftrightarrow$ 6s $^1S_0$ transition was one of the first atomic absorption spectra[1] to be obtained with the matrix-isolation technique. Spectra recorded[2] since the pioneering work of McCarty and Robinson[1] showed a three-fold split band for Hg/Xe in the vicinity of the gas phase transition at 253.7 nm while featureless bands, progressively blue-shifted from the gas phase transition, were observed in Kr and Ar matrices. In more recent times, luminescence was recorded and analyzed by the Orsay group[3] who used dye laser excitation of the 6p $^3P_1$ state and observed multiple emission bands in the UV for the rare gas (RG) matrices, Ar, Kr, and Xe. Although excitation spectra were not presented in this work,[3] the most intense emission bands had the smallest Stokes' shifts and were attributed to the occupancy of atomic mercury in substitutional sites. More recently, Chergui and co-workers[4] have conducted spectroscopic studies in neon matrices. Luminescence studies were extended by the Maynooth group,[5] who recorded excitation spectra and examined the temperature dependence of the observed emission.

In all these studies, the emission bands recorded for Hg/Xe were found to be distinct from those recorded for Hg/Kr, Hg/Ar, and Hg/Ne. Specifically, the Stokes' shift was much larger and the emission bandwidth was much greater than in the lighter rare gases. From a knowledge of the interaction potentials, derived from gas phase spectroscopic studies of the Hg·RG van der Waals diatomics,[6] this behavior was attributed to the formation of a strongly bound Hg·Xe exciplex. Preliminary experiments done by the Orsay group[3] on Hg/Ar doped with small amounts of xenon revealed emission in the vicinity of bands present in neat Hg/Xe samples. The results obtained in these mixed matrices supported the idea of exciplex formation in Xe/Ar samples. In the present study, we investigate this proposal in greater depth by recording the luminescence spectroscopy of Hg atoms in Ar matrices doped with varying amounts of Xe. Since the spectroscopic work done on atomic Hg in pure rare gas matrices has been reviewed,[7,8] only those aspects of the Hg/Ar and Hg/Xe systems relating to the behavior of mixed Hg·$(Xe)_n$ in Ar matrices will be addressed here.

Special Issue: Markku Räsänen Festschrift

Received: June 30, 2014
Revised: September 18, 2014

   dx.doi.org/10.1021/jp5065038 | J. Phys. Chem. A XXXX, XXX, XXX−XXX

Molecular dynamics calculations with quantum transitions (MDQT) have been used to examine the behavior of excited $^3P_1$ state Hg atoms in solid Ar,[9] confirming the substitutional site attribution made in the experimental[3,7] study. Recently, the theoretical studies have been extended by the Havana group[10] to cover all four rare gases Ne−Xe. These simulations showed the formation of exciplexes in the Hg/Xe system, but surprisingly, only complexes containing two Xe atoms were found to be the most stable excited state species, even in pure xenon. Specifically, two geometric forms of the excited $Hg(Xe)_2$ species were identified[10] in the calculations, one linear, the other with an angle of 150°. In agreement with the multicomponent nature of the experimental emission band, the two geometries were found to emit at different energies, with the linear form emitting at higher energy.

This report presents a combined experimental and theoretical study of the absorption and emission of the $^3P_1 \rightarrow {}^1S_0$ transition of atomic mercury isolated in solid Ar doped with small amounts of Xe. Particular attention is given to identifying the stoichiometry of the exciplex species in these mixed matrices. MDQT is used to follow the formation of exciplexes in simulated samples and to reproduce absorption and emission spectra. After a short presentation of the experimental and theoretical methods, experimental results and calculations are reported separately. The comparison between experimental and simulated spectra allows a precise analysis of the atomic arrangement around the trapped mercury, responsible for the observed spectroscopic features. The experimental data are discussed in light of the theoretical simulations in the last part of the article.

II. METHODS

II.1. Experimental. The thin film Hg/RG (RG = Ar and Xe) samples investigated in this work were prepared, as described elsewhere,[5] by co-condensing Hg vapor with the host gas of interest onto a CaF_2 window at a minimum temperature of 12 K. This temperature was achieved with an APD Cryogenics closed-cycle helium displex system (model HC-2) and was, unless otherwise stated, used to record all the scans presented. Selected samples were deposited at elevated temperatures of 22 and 35 K for Ar and Xe, respectively, to reduce the formation of thermally unstable sites. The temperature was monitored with a Scientific Instruments 9600-1 silicon diode mounted on the copper holder of the CaF_2 window. Samples containing known amounts of Xe in Ar were prepared in a dedicated gas handling system (GHS) maintained at vacuum in the low 10^{-8} mBar range by a Pfeiffer-Balzers turbomolecular (TPU-180H) pump. The amounts of the two rare gases in the GHS were monitored by two baratron gauges (Tylan General CDLD-11 and 31) sensitive in the ranges 0−10 and 0−1000 Torr, respectively. This allowed the dilution ratio of Xe in Ar to be known precisely. Samples were formed with gas flow rates of between 8−10 mmol/h by condensing onto the CaF_2 window at a set temperature. Using a previously described[5] "pick-up" method, in which Hg vapor at room temperature is entrained in the flowing host gas, deposition times of less than 30 min were sufficient to produce moderately absorbing Hg/(Xe)Ar matrix samples (OD = 0.9). The optical arrangements, both steady-state and time-resolved, used to conduct the spectroscopic measurements presented herein have been described[5] in detail already.

II.2. Calculations. *a. Samples.* The calculations described in this work were conducted with periodic boundary conditions pertaining to a system composed of 1 mercury atom and 499 rare gas atoms. The composition of the mixed Xe/Ar samples studied varied according to the number of Xe atoms included in the computational cell. Thus, 499-*n* Ar atoms and *n*Xe atoms were used, where *n* took the values 0, 1, 2, and 3. This number of RG atoms corresponds to a box large enough (5 times the lattice parameter of the *fcc* lattice) to avoid size effects, at least on the short timescales of the dynamical simulations. Drawing from results obtained in previous experimental[3,5] and theoretical work[9−11] done on pure matrices, the Hg atom was placed in a single substitutional site of the argon/xenon matrix. No other matrix site occupancies were explored in the present study.

Simulations were conducted by varying the number of Xe atoms, *n*, in the first $[nSS_1]$ and second $[nSS_2]$ solvation shells (SS) (i.e., the two shells of nearest neighbors Ar atoms around the guest Hg atom). When $n = 0$, the system consists of a mercury atom embedded in a pure argon matrix. In the case of $n = 1$, two situations were explored, namely $[1SS_1]$, which represents the xenon atom in the first shell, and $[1SS_2]$, in the second shell. The cases considered for $n = 2$ were $[2SS_1]$, $[2SS_2]$, and $[1SS_1\text{-}1SS_2]$ corresponding, respectively, to both xenon atoms in the first shell, both in the second shell, and one xenon in both the first and second shells. The four possible arrangements that exist for two Xe atoms in the first shell $[2SS_1]$ are based on the positions of the 12 nearest neighbors to the guest atom in a cuboctahedral substitutional site of the *fcc* lattice. The different possible arrangements for $[2SS_1]$, arising from having 2 Xe atoms placed in sphere 1, are labeled according to the characteristic angle (α) formed between the two directions that contain a Xe atom and atomic Hg. The values of α for the 4 different cases are, as depicted in Figure 1, 60°, 90°, 120°, and 180° corresponding to 4, 2, 4, and 1,

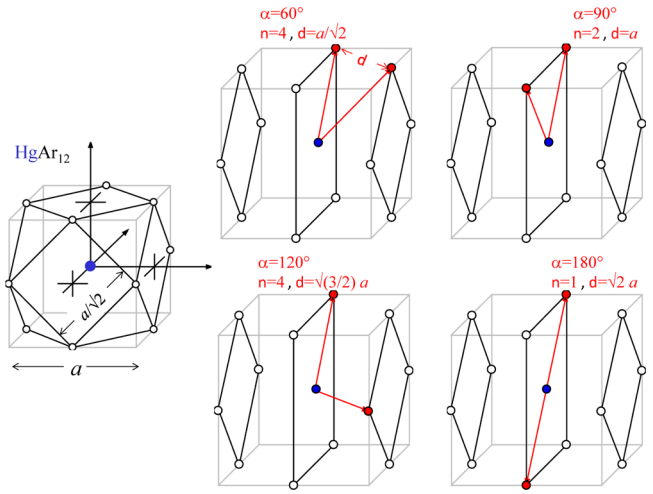

Figure 1. Diagram showing all possible arrangements that exist for two Xe atoms in the first sphere surrounding (SS) a Hg atom in a substitutional site of solid argon, $Hg/Ar_{10}Xe_2$ or using the current notation, $[2SS_1]$. The four arrangements are distinguished by the angle (α) formed between the two directions that contain a Xe atom and the Hg atom. The values of α for the different cases are 60°, 90°, 120°, and 180° with characteristic Xe−Xe distances (d) of $a/\sqrt{2}$, a, $\sqrt{(3/2)}a$, and $\sqrt{2}a$, respectively, where a is the lattice parameter of the *fcc* unit cell. The number of times (n) a given arrangement arises is also provided. The cuboctahedral symmetry Hg/Ar_{12} species, arising for the guest Hg atom in the *fcc* Ar lattice, is shown for comparison on the left.

dx.doi.org/10.1021/jp5065038 | J. Phys. Chem. A XXXX, XXX, XXX−XXX

respectively, possible arrangements. For n = 3, only the situations [$2SS_1$-$1SS_2$] and [$3SS_1$] were examined. In a similar way, all the different arrangements (a total of nine), in which three Xe atoms are located in the first shell [$3SS_1$], were considered.

b. Potential Energy Surfaces. All the interactions occurring between atoms in the sample are described in terms of pair-potentials. In its diatomic RG-Hg form, the $^3P_1$ state of atomic mercury splits into two states, namely $^3\Pi$ and $^3\Sigma$, differing by the projection of the excited orbital angular momentum onto the interatomic axis and by their bonding energies. Further mixing occurs due to spin−orbit coupling, which gives rise to the $A|0^+\rangle = |^3\Pi\rangle$ and $B|1\rangle = (|^3\Pi\rangle + |^3\Sigma\rangle)/\sqrt{2}$ stationary states. The A electronic state is allocated to the $|J = 1, \Omega = 0\rangle$ basis arising from the projection Ω = 0 of the mercury electronic angular momentum, J = 1 onto the interatomic axis. Correspondingly, the B state is allocated to the $|J = 1, \Omega = 1\rangle$ state of the complex.

Experimentally deduced potential energy curves, $V_A(R)$ and $V_B(R)$,[12,13] are used for these excited state interactions whose Morse parameters are quoted in Table 1 together with the potentials used for the ground state, V_X. The RG−RG interactions are described by the Lennard-Jones pair-potentials[14,15] given in Table 1, and the resulting potential energy curves are shown in Figure 2.

Table 1. Parameters of the Morse Functions Used to Provide the Potential Energy Curves of Hg−RG in the Ground X State and the A and B Excited States, Denoted by V_X, V_A, and V_B, respectively[a]

	D_e (cm^{-1})	β (Å^{-1})	r_e (Å)
Ar−Hg(X)[12]	130	1.448	3.98
Ar−Hg(A)[12]	354	1.541	3.34
Ar−Hg(B)[12]	52	1.116	4.66
Xe−Hg(X)[13]	254	1.249	4.25
Xe−Hg(A)[13]	1380	1.585	3.15
Xe−Hg(B)[13]	187	0.771	4.47
		ε (cm^{-1})	σ (Å)
Ar−Ar[14]		84	3.40
Xe−Xe[14]		161	3.98
Ar−Xe[15]		136	3.65

[a]The Lennard-Jones parameters ε and σ used to describe the potential energy curves of RG−RG dimers are also provided.

The total interaction Hamiltonian, H^{Hg-RG}, for the electronic states correlating asymptotically to Hg($^1S_0$) or Hg($^3P_1$) is obtained as the sum of pairwise interactions.

$$H^{Hg-RG} = \sum_{k=1}^{n_{RG}} H^{Hg-RG_k} \quad (1)$$

Due to the isotropic nature of the interactions with the Hg ($^1S_0$) atom, the ground state energies are obtained from eq 1 by a simple summation. However, in the excited states, involving an electronic angular momentum different from zero, where the quantization axis cannot be defined simultaneously along each Hg−RG bond, we have to write eq 1 with a common quantization axis. To achieve this, we followed the method presented by Bastida et al.[16] and Zuniga et al.[12] based on the use of Wigner rotation matrices, giving the matrix elements of H^{Hg-RG} between the $|J, \Omega\rangle_Z$ electronic wave functions of the mercury atom with projection Ω onto the Z axis. The use of the J, Ω basis seems appropriate because of the large spin−orbit coupling in the Hg−RG pairs. We then diagonalize the resulting diabatic matrix of H^{Hg-RG} in order to obtain the adiabatic energies E_i. Details of the practical implementation of this procedure are given in the appendix of ref 9. Potential energy surfaces (PES) are thus obtained from these energy calculations for the configurations of interest; in particular, the relaxed system in the ground state is used for absorption and the relaxed system in the excited state for emission.

c. Molecular Dynamics. The current calculations were carried out using a molecular dynamics with quantum transitions (MDQT) method.[17] In this approach, the electronic degrees of freedom are treated quantum mechanically, while the motions of the nuclei are treated classically. The movement of the nuclei is driven by the PES which, at a given time, is defined by a single electronic state. Hops from one electronic state to another are governed by the coefficients of the electronic wave function, determining at each time the elements of the electronic density matrix.[17,18] The diagonal elements of this matrix are proportional to the population of the electronic states involved.

As the first step in our calculations, the system was equilibrated in the electronic ground state for 200 ps at an

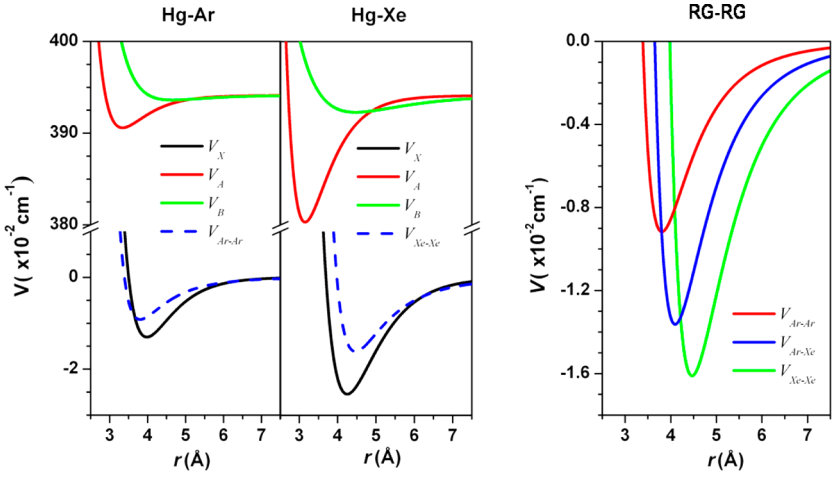

Figure 2. Potential energy curves of Hg−RG interactions for the ground state X and the A and B excited states, denoted by V_X, V_A, and V_B, respectively, and RG−RG interactions deduced from parameters reported in Table 1.

dx.doi.org/10.1021/jp5065038 | J. Phys. Chem. A XXXX, XXX, XXX−XXX

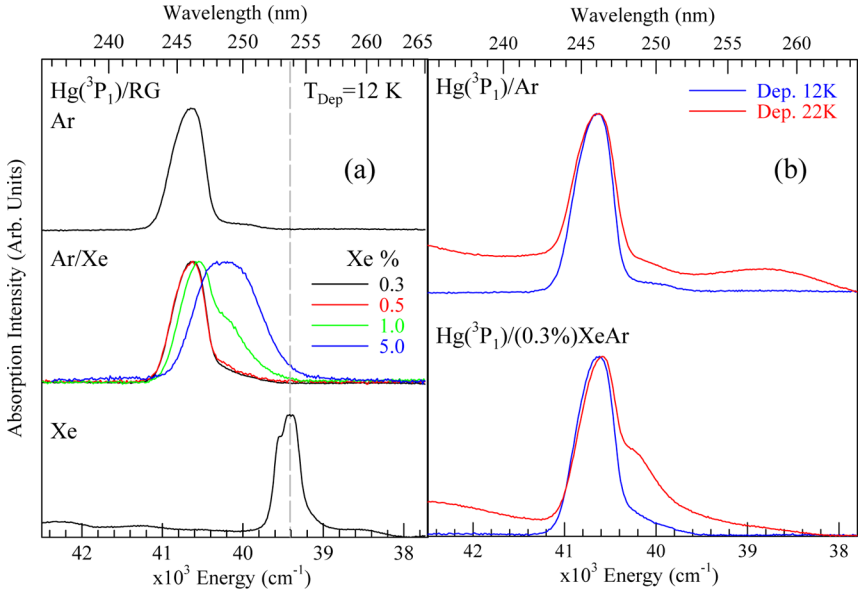

Figure 3. (a) Absorption spectra recorded at 12 K for the pure Hg/Ar and Hg/Xe systems and a comparison of the band shapes obtained with the specified amounts of xenon added to argon; the dashed vertical line provides the gas phase position of the Hg atom $6p^3P_1 \leftarrow 6s^1S_0$ transition at 39412.237 cm^{-1} (253.72 nm);[21] all the samples were deposited at 12 K. (b) Effects of deposition temperature on the clustering of xenon atoms around the Hg atom.

effective constant temperature (T′) of 49 K for Ar/Xe matrices. This value was obtained following the procedure described in ref 19 and selected so that the classical probability distribution for the atomic rare gas motions at T' equals the quantum probability distribution at the actual experimental temperature for solid Ar. A Debye cutoff frequency (ω_D) of 66 cm^{-1} was used in this estimation. Because of the low Xe concentrations used, it was assumed that the properties of pure Ar matrix remained unchanged in the mixed Ar/Xe matrices which have 499-n Ar atoms and nXe atoms for n = 1, 2, and 3.

Equilibrated trajectories in the ground electronic state were used to collect a set of initial positions and momenta (configurations) for the subsequent simulations in the excited states. The stored configurations fulfill the classical Franck–Condon principle for the electronic transition from the ground state to one of the three possible adiabatic excited states (energies, E_i) asymptotically correlated to $Hg(^3P_1)$. One hundred trajectories, all with a duration of 10 ps, were run from these initial configurations by vertical switching to each of the three excited states. This propagation time was found to be sufficient to achieve convergence of the final electronic state populations. During the course of the dynamics, the atom velocities were adjusted to the effective temperature, T', following the method described in ref 20.

The simulated lineshapes were obtained using the classical Franck–Condon approximation, in which the intensity of a given vertical transition is proportional to the residence time of the system in the neighborhood of the corresponding atomic configuration. Specifically, the spectra were calculated as histograms of the energy differences between the initial state (ground state for absorption, lowest excited adiabatic state for emission) and the final state (excited adiabatic states for absorption, ground state for emission), which implicitly takes into account the instantaneous gradient of the final state potential.

Spectra were produced from the contributions of $Hg(^1S_0)$ being in the distinct environments created by the presence of different numbers n = 0, 1, 2, and 3 of xenon atoms placed in the first and/or the second shells. Absorption spectra are obtained from 4000 configurations extracted from a single trajectory in the relaxed ground state. Emission spectra are obtained from configurations extracted from the 300 calculated trajectories (400 configurations per trajectory) after relaxation in the excited adiabatic state.

III. RESULTS

III.1. Recorded Spectra. The absorption spectra recorded for Hg atoms isolated in pure Ar and pure Xe matrices are shown on the top and bottom panels, respectively, in Figure 3a. A red shift of around 1200 cm^{-1} is observed from Ar (40670 cm^{-1}, 246 nm) to Xe (39430 cm^{-1}, 253.5 nm), as previously documented.[3,5] In the middle panel of Figure 3a, the absorption spectra recorded for Hg/Ar samples doped with Xe in amounts varying from 0.3 to 5.0% are shown. A red shoulder is present in samples containing 1% Xe or less, while in 5% Xe, a broad band, intermediate in position between pure Ar and pure Xe, is observed at ∼40100 cm^{-1} (∼249 nm). The absorptions of the 0.3 and 0.5% samples are quite similar but do differ slightly in the intensity of the red wing at 249 nm. All of the spectra shown in Figure 3a were deposited at 12 K. In Figure 3b, the effect of an elevated deposition temperature is presented for a 0.3% Xe/Ar mixture. By comparing with Figure 3a, it is evident that the 22 K deposited sample has a spectral shape strongly resembling the 1.0% Xe/Ar mixture deposited at 12 K. This clearly shows that the formation of xenon aggregates in the vicinity of the Hg atom is greatly enhanced at higher deposition temperatures. It is thereby a strong indication of nonstatistical isolation of xenon atoms in these Hg/Ar samples.

Emission spectra produced with wavelength-selected lamp excitation of the Hg atom absorptions are presented in Figure 4 (panels a and c) for pure Ar and pure Xe, respectively. That recorded in mixed matrices is shown in the central region (Figure 4b). It is immediately evident that the addition of 5% Xe to Ar matrices already produces intense, strongly shifted

dx.doi.org/10.1021/jp5065038 | J. Phys. Chem. A XXXX, XXX, XXX–XXX

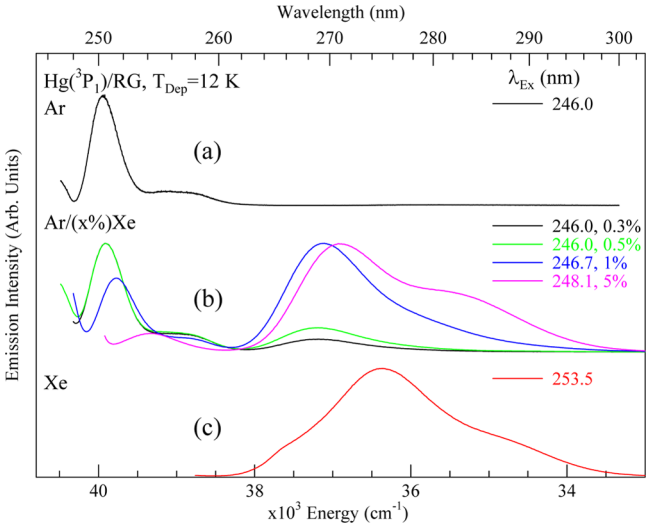

Figure 4. Details of Hg emission recorded at 12 K for the pure (a) Hg/Ar and (c) Hg/Xe systems and (b) in Ar samples doped with specified amounts of Xe.

emission bands in the same region as observed for pure Xe. On reducing the xenon concentration by a factor of 10 (to 0.5%), it is clear that the pure Ar emission at 39950 cm^{-1} (250 nm) dominates, but a single emission band remains at 37170 cm^{-1} (269 nm) whose intensity depends on the xenon content. It should be noted that the broad features located between 38500 and 39500 cm^{-1} are residuals of a thermally unstable site present in pure Ar. See trace (a) recorded in pure Ar for a comparison.

To examine the origins of the emission features shown in Figure 4b for the mixed Xe/Ar matrices, site-selective excitation spectra were recorded for a 0.3% sample, the results of which are presented in Figure 5. To minimize contributions from the thermally unstable site in Ar, these samples were deposited at 22 K. The excitation/emission spectra shown in the central panel (Figure 5b) reveal that the main Hg−Xe species absorb at 40500 cm^{-1} (247 nm) and emits at 37200 cm^{-1} (269 nm). The

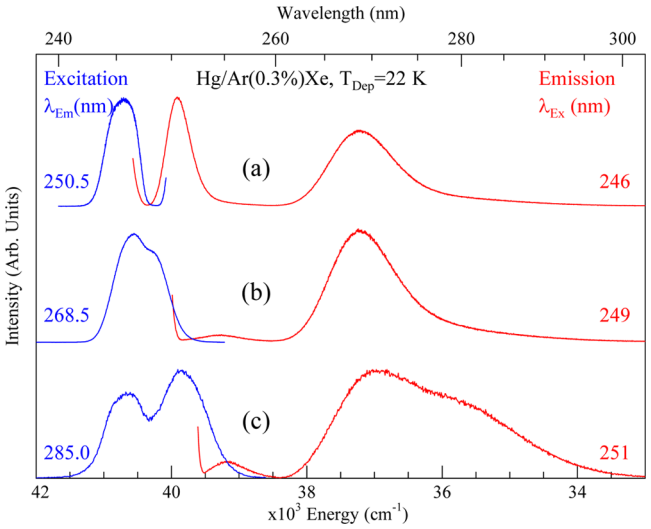

Figure 5. Excitation and emission spectra of a Hg/Ar sample doped with 0.3% Xe. The sample was deposited at 22 K, but the scans were recorded at 12 K.

reason that Hg in pure Ar sites contribute to the Hg−Xe emission at 37200 cm^{-1} becomes clear in the spectra shown in Figure 5a. It arises due to the efficient reabsorption of the pure Ar emission at 39950 cm^{-1} by the Hg−Xe absorption. Time-resolved emission spectra recorded with nanosecond dye laser excitation confirm this effect. Thus, the Hg in pure Ar emission at 39950 cm^{-1}, produced with direct excitation at 40650 cm^{-1}, has a decay time of 44 ns at 12 K. The corresponding Hg−Xe species emitting at 37500 cm^{-1} (267 nm) has a decay time of 50 ns when produced directly with excitation at 40200 cm^{-1} (248.7 nm), but when this emission is produced indirectly, with excitation at 40550 cm^{-1} (246.6 nm), it has a double exponential decay with the same 50 ns decay component. But in addition, it has a rise time of around 40 ns (the recorded emission decay profiles are presented in Figure S1 of the Supporting Information). This is a clear indication of radiative energy transfer arising from the spectral overlap of the distinct sites/species. In Figure 5c, an excitation scan of the emission feature furthest to the red, at 35000 cm^{-1} (285 nm), is shown. It consists of two components, the pure Ar band at 40650 cm^{-1} and a stronger band at 39980 cm^{-1}. The pure Ar component is also due to reabsorption, similar to the previous case. The other band reflects absorption of sites containing more Xe atoms in the surrounding of Hg than in the previous case (Figure 5b). The photophysical characteristics of the absorption and emission bands of Hg atoms in pure Ar, pure Xe, and mixed Xe/Ar samples are collected in Table 2.

III.2. Calculations. The large Stokes' shifts observed in mixed Xe/Ar matrices strongly suggest the formation of exciplexes with mercury for the most red-shifted emissions. This is similar to the case of Hg isolated in pure Xe matrices.[3,5] Consequently, detailed calculations are focused on situations where atomic xenon is present in the first surrounding shell (i.e., the $[1SS_1]$ and $[2SS_1]$ arrangements). The effects of Xe atoms in the second shell or additional to two Xe atoms in the first shell are only briefly described.

a. Equilibrium Configurations. In order to ascertain the disorder that xenon atoms may create in the Ar matrix and understand the mechanisms that drive the formation of exciplexes when the mercury atom is electronically excited, the relative position of Xe in the first shell was first analyzed in the ground state of the system.[10] The structural properties of the system were examined by calculating the radial distribution functions, g(r), of the surrounding rare gas atoms with respect to the mercury atom. The g(r) curves presented in the $[0SS_1]$ and the $[1SS_1]$ situations are the averages of 300 configurations for both the equilibrated ground state and the excited states. In the case of $[2SS_1]$, the radial distribution functions g(r) calculated are the average of 1200 configurations for both ground and excited states.

In pure Ar matrices, the presence of ground state atomic Hg only perturbs the lattice locally by expanding the first shell around 0.09 Å, as shown in Figure 6a. This expansion increases to 0.13 Å when there is one Xe atom in the first solvation shell (Figure 6b) and is only slightly more pronounced when there are two Xe atoms in this shell, corresponding to a more perturbed arrangement (Figure 6c). The structure of the extended matrix is largely unchanged [see red dot-dash lines in Figure 6 for g(r) RG−RG, compared to blue dash lines], which means that the perturbation caused by the introduction of the Hg and Xe atoms on the Ar lattice is weak and localized.

Excitation of atomic Hg to the $^3P_1$ state changes the electronic properties of the guest atom dramatically with the

dx.doi.org/10.1021/jp5065038 | J. Phys. Chem. A XXXX, XXX, XXX−XXX

Table 2. Photophysical Characteristics of the 6p $^3P_1 \leftrightarrow$ 6s $^1S_0$ Transition of Atomic Mercury Isolated in Matrices Containing Specified Amounts of Xenon (Experiments) or in Specified [nSS_1] Environments (Simulations)[a]

experiments				simulations		
	absorption	emission			absorption	emission
Hg/RG system	ν_{ABS}/Δ (cm^{-1})	ν_{em}/Δ (cm^{-1})	SS (cm^{-1})	Hg/RG system	ν_{ABS}/Δ (cm^{-1})	ν_{em}/Δ (cm^{-1})
Ar	40670/480	39950/400	720	Ar	40320/420	39710/460
Xe	39430/340	36360/1470	3070	Xe	38730/280	34540/2040
% Xe/Ar						
5	40160/900	36900/1500	3260	$3SS_1$	39670/600	36710/1390
		35460/1800	4700			34210/1960
1	40480/500	39790/450	690	$2SS_1$	39890/550	36790/1290
	40160_{sh}/–	37170/1470	2990			34480/2040
<0.5	40670/480	39950/400	720	$1SS_1$	40080/480	36890/1250
	40160_{vwsh}/–	37170/1470	2990			

[a] ν_{ABS} corresponds to the central component of the three-fold split absorption band, while ν_{em} indicates the emission band center. The full width at half-maximum intensity of the bands is denoted by Δ and the Stokes shift by SS. All values are in wavenumber (cm^{-1}) units. The abbreviations "sh" and "vwsh" indicate a shoulder and a very weak shoulder, respectively. The experimental values are extracted from the spectroscopy of samples deposited at 12 K.

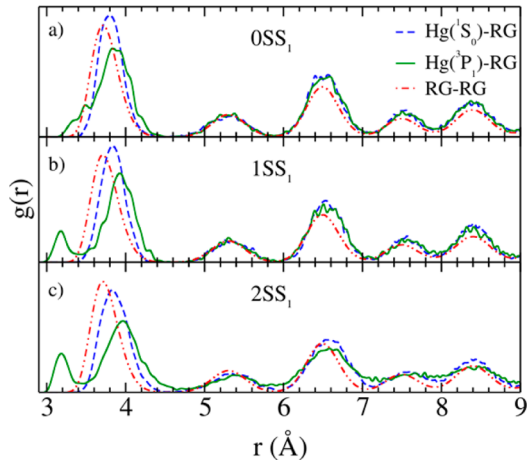

Figure 6. Radial distribution functions for cases (a) [$0SS_1$], (b) [$1SS_1$], and (c) [$2SS_1$] in the ground state (blue dashed curves) and in the excited state (green curves). Red dot-dash curves correspond to samples without mercury impurities.

guest–host interaction becoming highly anisotropic. While the system is stabilized in the excited state, the g(r) Hg($^3P_1$)-RG curves (full green lines in Figure 6) show different profiles in the first solvation shell. In pure Ar matrices [$0SS_1$], the plots exhibit an additional displacement of about 0.05 Å and a nonsymmetric broadening (Figure 6a). The left side of the band presents a complex structure corresponding to two Ar atoms that are closer to the mercury atom than the others. This behavior was previously found for Hg in pure argon as shown in Figure 4 of ref 10. When the first solvation shell contains Xe atoms, the g(r) plots (Figure 6, panels b and c) of the excited Hg($^3P_1$)-RG state reveal a splitting of the first band in two. In the [$1SS_1$] arrangement, the main band represents an expansion of this shell by about 0.1 Å with respect to its position in the ground state, while the minor band at short range is related to the formation of Ar–Hg($^3P_1$)–Xe exciplexes. The latter band is located at 3.19 Å and arises from the excited molecular complex formed between the Xe atom, the excited Hg($^3P_1$) atom, and an Ar atom in a linear arrangement. It is noteworthy that this value is, as quoted in Table 1, very similar to the bond length of the excited A state of HgXe. In the [$2SS_1$] arrangements, the minor band of the splitting corresponds to the formation of Ar–Hg($^3P_1$)–Xe and Xe–Hg($^3P_1$)–Xe exciplexes. The Ar–Hg($^3P_1$)–Xe complex also has a linear conformation as was observed for the [$1SS_1$] case, but the Xe–Hg($^3P_1$)–Xe complexes exhibit both linear and nonlinear geometries.

As described in Methods, four distinct arrangements exist for [$2SS_1$] whose contributions to the g(r) curve were weighted according to the geometrical probabilities (n values given in Figure 1) of finding the ground state arrangements [$2SS_1$] with different values of α. Figure 7 shows the g(r) curves calculated

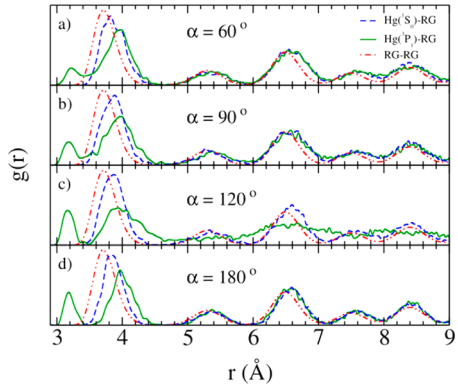

Figure 7. Radial distribution functions for the case [$2SS_1$]. (a) $\alpha = 60°$, (b) $\alpha = 90°$, (c) $\alpha = 120°$, and (d) $\alpha = 180°$, in the ground state (blue dashed curves) and in the excited state (green curves). Red dot-dash curves correspond to samples without mercury impurities.

for each case of α and averaged from 300 configurations. In all four cases, the first band is split in two after excitation of the mercury atom. With the exception of $\alpha = 120°$ case, the longer range structure of the g(r) Hg($^3P_1$)-RG bands is maintained for [$2SS_1$] arrangements. In the case of $\alpha = 120°$, the loss of structure that occurs in the distant shells arises because the Hg atom has moved out of its initial central position (see below) at equilibrium. Formation of the Ar–Hg($^3P_1$)–Xe exciplex is observed for $\alpha = 60°$ and $\alpha = 90°$, a temporary Xe–Hg($^3P_1$)–Xe can also be formed for $\alpha = 90°$, while only the Xe–Hg($^3P_1$)–Xe molecular complex is found for α values of 120° and 180°. In all the [$1SS_1$] and [$2SS_1$] arrangements, the matrix preserved its properties after the excitation of the guest atom, and the deformation is localized and weak.

dx.doi.org/10.1021/jp5065038 | J. Phys. Chem. A XXXX, XXX, XXX–XXX

In summary, the equilibrium geometries of the exciplexes formed in [$1SS_1$] are linear Ar−Hg−Xe exciplexes, d(Ar−Hg) ∼ 3.55 Å, and d(Xe−Hg) ∼ 3.20 Å. This geometry is also present in [$2SS_1$] for the α = 60° and 90° arrangements. In the stabilized Ar−Hg*−Xe exciplex, the Hg−Ar bond length is greater than the Hg−Xe bond length but shorter than the value in the ground state (3.83 Å). The Xe−Hg−Xe exciplex present in [$2SS_1$] has the same Xe−Hg bond length (3.20 Å) for α = 120° and 180°, with a linear geometry in the latter situation and an angle of 140° in the former. In comparison, d(Xe−Hg) = 3.28 Å in the Xe−Hg*−Xe exciplexes formed in pure Xe matrices, highlighting the environment effect on the structure of these exciplexes, and d(Ar−Hg) = 3.44 Å was obtained for Ar−Hg*−Ar linear structures in pure Ar,[10] showing the effect of attractive forces between Hg* and Xe on the Hg*−Ar bond length.

b. Dynamics in the Excited States. The initial position corresponds to a vertical transition from the stabilized ground state (i.e., from the geometry of the lattice where Hg is in the center of a substitutional site), with only the first shell around it weakly perturbed (Figures 6 and 7). Surface hopping between the adiabatic excited states takes place in the very beginning dynamics, and the lowest excited state is reached within the first 3.5 ps. These time intervals increase as a function of the number of Xe atoms surrounding the Hg, being 1 ps for n = 0 (pure Ar), 1.7 ps for n = 1, and 3.4 ps for n = 2. The dynamics of the formation of exciplexes were then investigated by analyzing the atomic trajectories in the excited states in a 10−20 ps time range.

With only one Xe in the first shell, the formation of a linear Ar−Hg($^3P_1$)−Xe exciplex results from the concerted motions of xenon and the colinear argon atom toward the central Hg atom, as shown in Figure 8. One can notice in Figure 8 that the equilibrium configuration is reached in less than 2 ps, consistent with the population relaxation time of 1.7 ps obtained for this

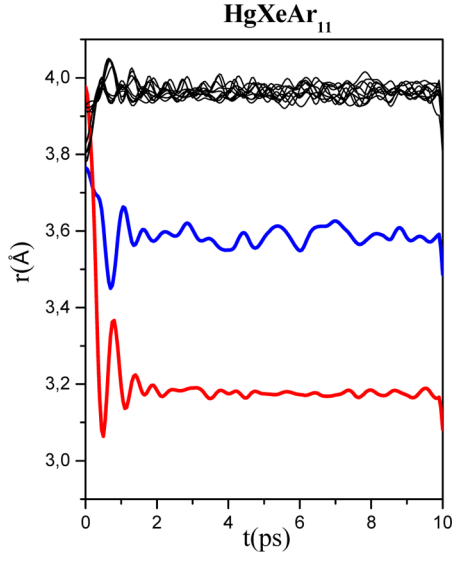

Figure 8. Time evolution of distances between mercury and each of the 12 nearest neighbors of the first solvation shell in [$1SS_1$] arrangements in the first ps following the excitation of Hg. Trajectories were calculated at 49 K and the solid lines represent the average of 300 trajectories. d(Hg*−Xe), red; d(Hg*−Ar) for the Ar atom in the linear Xe−Hg−Ar geometry, blue; and d(Hg*−Ar) for the 10 other Ar atoms, black.

arrangement, as mentioned above. With two Xe atoms in the first shell, the dynamics are more complex. Figure 9 presents

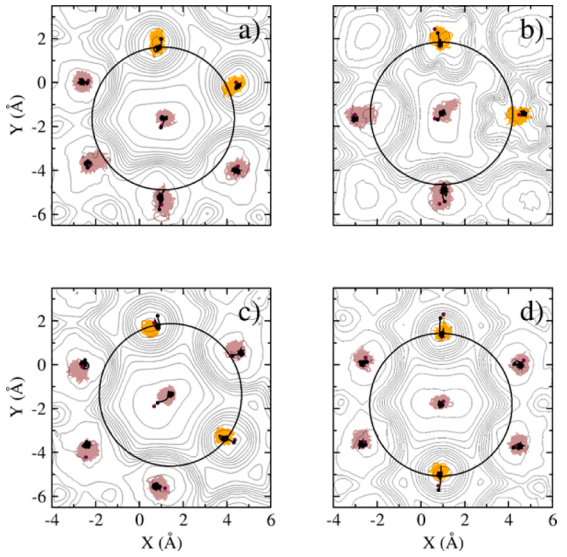

Figure 9. Trajectories of nearest neighbors to the Hg in a plane XY that contains this guest atom and two Xe atoms. (a) α = 60°, (b) α = 90°, (c) α = 120°, and (d) α = 180°. Hg is the center of each plot. In orange and brown, the trajectories obtained at 49 K are represented. The orange traces belong to the Xe atoms. Trajectories at 4 K are plotted as black lines for comparison. The small dots (solid circles) indicate the starting positions (black at 4 K, brown at 49 K). In all cases, the circle has a radius 3.25 Å and is centered in the position of Hg($^3P_1$) stabilized at 4 K. Contour lines of PES in the first excited adiabatic level in the stabilized configuration are added in gray lines.

examples of trajectories in the four cases of the angle α. Hg is in the center of each plot. Trajectories of Xe at 49 K (tracked for 200 ps) are represented in orange, while those of Hg and Ar are in brown. In order to reduce the fluctuations due to the thermal motion and simplify the trajectories, simulations have also been performed at 4 K. The corresponding trajectories are represented in black in Figure 9, highlighting the most probable positions. The large black circle centered on Hg in the excited state is drawn to emphasize Xe and/or Ar atoms which form the exciplex (those which have parts of their trajectories inside the circle). Moreover, Figure 9 presents cuts of the excited PES through the planes containing Hg and two Xe atoms for the four possible [$2SS_1$] arrangements. Complementary information on the trajectories is given in the Supporting Information, where Figure S2 presents plots of Hg−RG distances versus time for the 12 first neighbors. The data are shown for sample temperatures at 49 and 4 K.

When α = 60° (Figure 9a), it is evident that the two Xe atoms come close to the Hg atom at 49 K since their trajectories enter the circle of radius 3.25 Å. Less obvious, but very significant, the trajectories of the two Ar atoms which are on the opposite side of the Xe atoms also show movement toward Hg. In this regard, it must be pointed out that the two Xe atoms do not approach or remain close to the Hg atom simultaneously, as shown by the trajectory at 4 K (see also the comparison between panels a and b of Figure S2 of the Supporting Information). Thus, at any particular time, what exists is the (Ar−Hg−Xe)* complex with a geometry very close to the exciplex obtained in [$1SS_1$] arrangements (see Figure 8

dx.doi.org/10.1021/jp5065038 | J. Phys. Chem. A XXXX, XXX, XXX−XXX

and Figure S2 of the Supporting Information, panel a at 4 K and panel b at 49 K).

The $\alpha = 90°$ case (Figure 9b) presents many similarities with that of 60° inasmuch as a well-defined interchange mechanism exists between the two Xe atoms forming the complex. The alternate formation of the two Ar−Hg−Xe species continues for long periods of time during all dynamics at 49 K, whereas only one complex is clearly observed at 4 K. Additionally, at 49 K, Xe−Hg($^3P_1$)−Xe exciplexes are formed for much shorter periods, corresponding to motion of Hg toward the middle of Xe−Xe. This is presented in Figure S2 of the Supporting Information, panel d, to be compared with the "frozen" situation (panel c). These Xe−Hg($^3P_1$)−Xe exciplexes do not correspond to equilibrium geometries, and their contributions to the calculated g(r) curves presented in Figure 7 are small.

With $\alpha = 120°$ (Figure 9c), trajectories are different because they show a pronounced motion of the Hg atom away from the center of the substitutional site toward the middle of the adjacent Xe−Xe pair. It does this in order to form the quasi-linear Xe−Hg($^3P_1$)−Xe exciplex. This explains the loss of structure highlighted in Figure 7c, green solid line. The apparent approach of the one Ar atom between the Xe pair to Hg for $\alpha = 120°$ is an artifact. It arises, as noted in the g(r) plots (Figure 7c), because of the extent of the migration (1 Å) of the Hg atom to the Xe pair. Finally, with $\alpha = 180°$ (Figure 9d), the formation of the linear Xe−Hg($^3P_1$)−Xe exciplex is clearly observed, at 49 K and at 4 K, with both Xe atoms simultaneously crossing the black circle. In the two last cases, only the (Xe−Hg−Xe)* complexes are formed in the dynamics irrespective of the temperatures involved (see Figure S2 of the Supporting Information, panels e−h).

The dynamical formation and evolution of the electronic excited molecular complexes shows the presence of several mechanisms also observed in previous work on the photo-excitation of Hg atom embedded in a pure Xe matrix.[10] The formation of complexes occurred in both sequential and concerted mechanisms for sites with two Xe atoms, but the latter is predominant and the only one observed in the formation of linear Ar−Hg($^3P_1$)−Xe complexes. The concerted mechanism is illustrated in Figure 8 for the [$1SS_1$] arrangement: thus when the guest Hg atom is photoexcited, the Xe atom comes close to it, pushing out the nearest Ar atoms in the direction of its movement. The displacement of these Ar atoms decreases their action on the Ar atom that is positioned in the first solvation shell in line with the Hg atom and the Xe atom. At the same time, the attractive forces acting on it are increasing because the Ar−Hg interaction becomes important. This behavior is also observed for sites with two Xe atoms [$2SS_1$] when $\alpha \sim 90°$ and 60° but alternating the formation of the Ar−Hg($^3P_1$)−Xe complex involving each Xe. An (Ar−Hg−Xe)* complex is formed then the Xe and Ar atoms come away while at the same time the other Xe atom and its Ar partner approach to form a new (Ar−Hg−Xe)* complex. This process continues in time as shown in panels (b and d) of Figure S2 of the Supporting Information.

c. Simulated Spectra. The contributions of the different $(Xe)_nAr$ arrangements to the absorption and emission bands are shown in Figure 10. The main characteristics of these bands are reported in Table 2. A red shift of 240 cm^{-1} is obtained in absorption from pure Ar [$0SS_1$] to the $(Xe)_1Ar$ [$1SS_1$] situation, whereas the shift increases to 2820 cm^{-1} in emission because of the formation of Ar−Hg($^3P_1$)−Xe exciplexes. In the [$2SS_1$] situation, the contributions of each of the Xe_2Ar_{10}

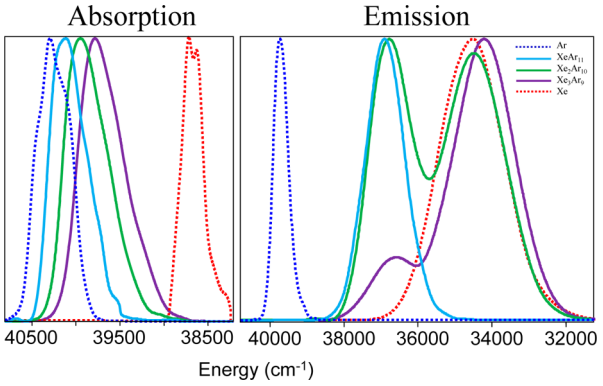

Figure 10. Simulated absorption (left) and emission (right) spectra for different arrangements: pure Ar, dot dark blue; one Xe in the first solvation shell, solid light blue; two Xe in the first solvation shell, solid green; three Xe in the first solvation shell, solid purple; and pure Xe, dot red. Simulations in light blue and green include one Xe in the second solvation shell.

arrangements to the absorption band are quite similar, and the resulting band exhibits no clear structure. In contrast, their contributions to the emission are different, resulting in a more complex spectrum with, as shown in Figure 10, two important components. The analysis in terms of α dependence shows that one of these components is associated with the formation of Ar−Hg($^3P_1$)−Xe exciplexes and is close to the previous [$1SS_1$] case and that the other band is associated with the formation of Xe−Hg($^3P_1$)−Xe exciplexes.

The influence of one Xe in the second shell [$1SS_2$] on the Hg atom is very weak. It has no effect on the position of the bands but does induce a slight broadening (mainly in absorption) due to greater disorder in the site structure. The spectra shown in Figure 10 include this effect. The addition of a third Xe atom in the first shell [$3SS_1$] induces a red shift of the absorption band (Figure 10). The emission presents the same two components, coming from the formation of linear or quasilinear Xe−Hg($^3P_1$)−Xe and Ar−Hg($^3P_1$)−Xe complexes in the excited state. The probability to form Xe−Hg($^3P_1$)−Xe exciplexes increases of course in this case. In mixed Xe/Ar matrices, linear and quasilinear Xe−Hg*−Xe exciplexes produce very similar emission bands, contrary to the case of pure Xe, where a shift of 580 cm^{-1} in the emission bands was calculated. This shift could be explained by the slightly different exciplex geometries obtained in the two cases, induced by the effect of different surroundings.

IV. DISCUSSION

Theoretical simulations are in good agreement with experimental results in terms of the formation of exciplexes and provide clear explanations of the observed spectroscopic data. A detailed comparison of the experiments and simulations will be made and examined in this discussion.

IV.1. Spectroscopy and Complex Formation. *a. Absorption.* Molecular dynamics results show that the position of the absorption band depends strongly on the number of Xe atoms in the first solvation shell [nSS_1]. Increasing the number of Xe atoms in SS_1 (n = 1−3) shifts the band toward the pure Xe matrix absorption band (Figure 10). The broadening and red shift observed in the experiments when increasing the amount of Xe in the Ar/Xe mixture (Figure 3) is thus mainly explained by the increase in the number of Xe atoms which are nearest

dx.doi.org/10.1021/jp5065038 | J. Phys. Chem. A XXXX, XXX, XXX−XXX

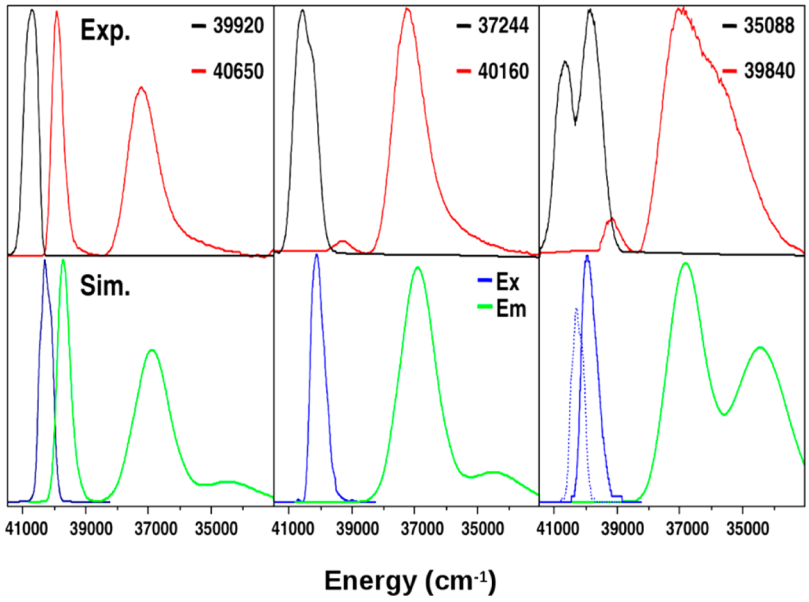

Figure 11. Comparison of the experimental and simulated spectra in the case of a 0.3% Xe/Ar mixture deposited at 22 K. The excitation spectra are shown in black and blue, while the emission spectra are in red and green. The dot blue line represents absorption in pure Ar, arising in excitation spectra because of energy transfers between sites (see Experimental Spectra). Experimental values of observation wavenumbers for excitation spectra (black lines) and of excitation wavenumbers for emission spectra (red lines) are given in inverse centimeters. The adjustments of the parameters required to reproduce experiments in the simulation are discussed in the text.

neighbors to Hg in the sample. When the Hg atom is in the ground $^1S_0$ state, no complexes with Ar or Xe were formed.

b. Emission. In the emission simulations, three distinct bands were obtained (Figure 10), which are assigned to the following three situations. The first corresponds to sites with the Hg surrounded by only Ar atoms. The second arises from the metal forming an Ar−Hg($^3P_1$)−Xe complex with one Xe atom in the first solvation shell. The last occurs when two Xe atoms are placed in the first solvation shell in specific geometries leading to the formation of a Xe−Hg($^3P_1$)−Xe complex.

In experiments, one can also distinguish three broad emission bands whose intensities show a strong dependence on the amount of Xe present but whose frequency positions (Figures 4 and 5) are only weakly concentration dependent. The good agreement with the experiment demonstrates that we are able to assign each band of the recorded emission spectrum to the formation of the molecular complexes described before. In Table 2 and Figure 11, it is evident that the contribution of the Hg atom in pure Ar [$0SS_1$] sites and the emission from Ar−Hg($^3P_1$)−Xe complexes are in better accord with experiments than the emission from Xe−Hg($^3P_1$)−Xe complexes. This phenomenon was also observed by Rojas-Lorenzo et al.[10] and may be due to the method and/or the parameters of the gas phase Hg−Xe pair-potentials used for the construction of the PES. One can notice by the way the present pure Xe calculated spectrum is red shifted in comparison with the one published in ref 10, where older parameters for the Hg−Xe pair potential were used.

The formation of linear triatomic exciplexes between the excited mercury and rare gas atoms is a consequence of the attractive Hg−RG interaction in the A state (Table 1 and Figure 2). The potential well is deeper for Xe than for the other rare gases, leading to a stronger interaction and a shorter Hg−RG equilibrium distance with Xe and, consequently, to a larger Stokes' shift between absorption and emission bands. The A ($A|0^+\rangle$, $|J = 1,\Omega = 0\rangle$) electronic state is nondegenerate for the Hg−RG diatomics, and only one of the three degenerate levels of Hg($^3P_1$) is involved in this molecular state. For symmetry reasons, the same orbital is involved in the attractive potentials with the two RG atoms in the RG−Hg−RG linear geometry. This explains the formation of linear exciplexes, even when an Ar atom is in the linear RG−Hg−Xe geometry instead of a Xe. These linear exciplexes were effectively formed with RG = Ar and Kr in the simulations described in ref 10, but as d[Hg($^3P_1$)−Ar] or d[Hg($^3P_1$)−Kr] are only slightly shorter than the equilibrium distances in a substitutional site of the lattice, the formation of such weak exciplexes do not lead to large experimental Stokes' shifts.[3,5] In the case of light metal atoms, M, such as Li or Na, with negligible spin−orbit interaction, the bound M(^2P)−RG pair potential (A state) corresponds to the doubly degenerate $^2\Pi_{1/2,3/2}$ states. This can explain qualitatively the results obtained theoretically in the latter case, whereby the excitation to M(^2P) in the rare gas matrix induces attraction with the surrounding RG atoms placed in a plane instead of a line as observed for Hg($^3P_1$).[22,23]

IV.2. Analysis of the Site-Selected Results. The experiments done on the Hg(Xe)/Ar samples reflect a mixture of [nSS_1] arrangements, with n = 0 to 12. In the low xenon concentration range explored in the present work, we can assume that the contributions of [$(n > 2)SS_1$] arrangements are negligible. As mentioned previously, emission occurs in three distinct spectral ranges, corresponding to (i) [$0SS_1$], (ii) [$1SS_1$], [$2SS_1$] with α = 60° or 90°, and (iii) [$2SS_1$] with α = 120° or 180°. Assuming that the probability of [$2SS_1$] with α = 60° and 90° is equal to that of [$2SS_1$] with α = 120° and 180°, one can extract the proportion of [nSS_1] arrangements (n=0, 1, and 2) from an experimental emission spectrum. To do this, we fit Gaussian functions to the experimental spectrum, and the area of each Gaussian function was related to the weight of each different contribution. This process, applied to the experiment with 0.3% Xe in Ar of Figure 5, gives the results shown in

dx.doi.org/10.1021/jp5065038 | J. Phys. Chem. A XXXX, XXX, XXX−XXX

Figure 11. Calculated emission spectra (green curves) are obtained taking into account the weight $W(n)$ of each $[nSS_1]$ (n = 0, 1, and 2) arrangement at the excitation wavelength estimated from the analysis of experimental spectra (red curves). The discrepancy that exists between the experimental and simulated spectra comes mainly from the red shifted calculated frequency of the Xe−Hg($^3P_1$)−Xe exciplex. When exciting in the red wing of the absorption spectrum (right panel), $[2SS_1]$ arrangements are mainly excited [$W(2)$ = 80%], and no Hg atom in a pure Ar environnement are excited [$W(0)$ = 0]. In contrast, when exciting in the main Hg/Ar absorption profile (left panel), the pure Hg*/Ar emission is observed and $W(0)$ = 33%; other weights are $W(1)$ = 49% and $W(2)$ =18%. The middle panel corresponds to the case of a strong Ar−Hg($^3P_1$)−Xe exciplex emission, with $W(1)$ = 74% and $W(2)$ = 26% [$W(0)$ = 0].

Excitation spectra at each of the three emission wavelengths are also calculated (Figure 11, blue curves), taking into account the weight of each $[nSS_1]$ (n = 0, 1, and 2) configuration at the emission wavelength, with the simplest cases $W(0)$ = 100% in the left panel and $W(2)$ = 100% in the right panel. Still assuming that $[nSS_1]$ arrangements with $n > 2$ do not exist, the probabilities $P(n)$ to get $[nSS_1]$ n = 0, 1, and 2 arrangements in the sample could be deduced from this analysis, taking into account estimated shifts between experimental and calculated frequency values. Simulations allow a semiquantitative understanding of the dependence of emission spectra on the excitation wavelengths used and vice versa, the dependence of excitation bandshapes on the emission wavelengths monitored.

IV.3. Statistics and Temperature Effect. In the example of Figure 11, the weights $W(n)$ obtained from the analysis of the left panel, corresponding to an excitation in the maximum of the absorption profile (see Figure 3b), are not far from the probabilities $P(n)$. It is obvious that these values do not correspond to a statistical distribution. Applying a simple statistical distribution, the probabilities to find the $[nSS_1]$ (n = 0, 1, and 2) environments in an Ar sample containing 0.3% Xe are calculated to be $P_S(0)$ = 96.5%, $P_S(1)$ = 3.5%, and $P_S(2) \sim 0$. As was pointed out already and shown in Figure 3b, the occurrence of Xe atoms in the first shell depends strongly on the deposition temperature. The shoulder that appears in the absorption spectra of the Hg/Ar doped with 0.3% Xe when the sample was deposited at 22 K can be explained in terms of the mobility of the Xe atoms. During deposition at this temperature, Xe atoms can migrate easily through the matrix and find a position closer to the Hg atoms. As a result, by increasing the deposition temperature, the sites with one or more Xe atoms in the first shell will be favored. The same effect was described in ref 3, Figure 5. This clearly means that the interaction between atoms cannot be neglected in the formation of the sample. From the pair-potential parameters used for the construction of the PES, it is evident that the Hg−Xe interaction is stronger than Hg−Ar, so that during the deposition process, Xe atoms will move closer to the Hg and the higher the deposition temperature, the more pronounced is this effect. In this regard, it should be remarked that for α = 60° in the $[2SS_1]$ arrangement, sample thermalization was difficult to achieve in the simulations because of the high repulsion between the two Xe atoms at a distance shorter than the equilibrium distance of Xe_2. This means that the amount of $[2SS_1]$ arrangements with α = 60° are probably overestimated in our simulations and simply implies an underestimation of $[1SS_1]$ arrangements but does not affect the estimation of $P(0)$, which is clearly lower than $P_S(0)$.

From the emission spectra, we are able to estimate the weight of each configuration and conversely we are able to simulate the emission spectrum of a sample applying a simple statistical distribution. Such a simulation in the case of 0.3% Xe in Ar shows that emission from Ar−Hg*−Xe exciplexes should be very weak (1.4%) when exciting in the maximum of the absorption band. It means that the emission spectrum reported in Figure 4 from samples deposited at 12 K does not correspond to a statistical distribution, even if this statistical distribution is more closely approached with a low-temperature deposition.

V. CONCLUSIONS

Absorption and emission spectroscopies were performed on mixed Ar/Xe matrices doped with mercury, highlighting the effect of a small amount of Xe on the formation of exciplexes. Molecular dynamics calculations done with the surface-hopping model help to assign the observed spectroscopic bands and have greatly improved the understanding of the formation of complexes in the excited state. The observed structure in the recorded emission bands has contributions from three different families of Hg atom matrix sites (i.e., pure Ar surrounding, possible formation of Ar−Hg*−Xe exciplexes, and possible formation of Xe−Hg*−Xe exciplexes). The presence of Xe in the mercury surrounding was also manifested in absorption but only as unresolved shoulders, without clear distinctions between these families of sites. Good agreement was found between the experimental and simulated spectra, indicating that the model is capable of describing in a very realistic way the interaction of the electronic ground and excited states of atomic mercury with its solid state environment.

The main result is the strongly preferred formation of linear triatomic exciplexes upon excitation of Hg in its $^3P_1$ state. The specific interaction between Hg and Xe was well-known, inducing red-shifted and broad emission bands in Xe matrices,[3,5] but simulations clearly showed that this interaction does not induce the formation of a diatomic XeHg exciplex in the matrix; instead a linear triatomic species is formed.[10] In the present case of mixed Ar/Xe matrices, such linear triatomic exciplexes are also formed, and if enough Xe atoms are not available in the right sites, they involve Ar atoms as nearest neighbors of the excited Hg. More sophisticated calculations are necessary to better simulate the emission bands of Xe−Hg($^3P_1$)−Xe exciplexes, but the main physical effects are well-reproduced.

■ ASSOCIATED CONTENT

Supporting Information

Figure S1: experimental emission lifetimes recorded at different wavelengths and upon different excitations in a Hg(Xe)/Ar sample. Figure S2: simulated time evolution of d(Hg*−RG) for RG in the first SS, in [2SS1] arrangements; a detailed explanation of the plot is given. This material is available free of charge via the Internet at http://pubs.acs.org.

■ AUTHOR INFORMATION

Corresponding Author

*E-mail: claudine.crepin-gilbert@u-psud.fr. Tel: +33 1 69 15 75 39.

dx.doi.org/10.1021/jp5065038 | J. Phys. Chem. A XXXX, XXX, XXX−XXX

Notes

The authors declare no competing financial interest.

■ ACKNOWLEDGMENTS

This research was funded by the Irish Government IRCSET Embark research grant 2006 to whom M.R. gratefully acknowledges receipt of a Ph.D. studentship. R.L.-G. and G.R.-L. acknowledge a scientific project supported by InSTEC. This work also benefited from funds given by the French embassy in Cuba and Région Ile de France (SETCI grant) for travel exchanges.

■ REFERENCES

(1) McCarty, M.; Robinson, G. W. Environmental Perturbations on Foreign Atoms and Molecules in Solid Argon, Krypton and Xenon. *Mol. Phys.* **1959**, *2*, 415−430.
(2) Laursen, S. L.; Cartland, H. E. Multiplicity Dependence of Matrix-Induced Frequency-Shifts for Atomic Transitions of the Group 12 Metals in Rare-Gas Solids. *J. Chem. Phys.* **1991**, *95*, 4751−4755.
(3) Crépin, C.; Tramer, A. Spectra and Relaxation Paths of Hg($^3P_1$) in Rare-Gas Matrices. *J. Chem. Phys.* **1992**, *97*, 4772−4780.
(4) Helbing, J.; Chergui, M.; Haydar, A. Spectroscopy and Energy Relaxation Processes of Hg-doped Solid Neon, Argon, and Xenon. *J. Chem. Phys.* **2000**, *113*, 3621−3632.
(5) Collier, M. A.; McCaffrey, J. G. Luminescence Spectroscopy of $^3P_1$ and $^3P_0$ State Atomic Mercury Isolated in Solid Ar, Kr, and Xe. *J. Chem. Phys.* **2003**, *119*, 11878−11887.
(6) Breckenridge, W. H.; Jouvet, C.; Soep, B., Metal-Atom/Rare-Gas Van der Waals Complexes. In *Advances in Metal and Semiconductor Clusters*, Duncan, M., Ed. JIA Press: Greenwich, CT, 1995; Vol. 3.
(7) Crépin, C.; Legay, F.; Legay-Sommaire, N.; Tramer, A. Spectroscopy, Dynamics and Photochemistry of Mercury Atoms in Low Temperature Matrices. *Trends Chem. Phys.* **1999**, *7*, 111−132.
(8) Crépin-Gilbert, C.; Tramer, A. Photophysics of Metal Atoms in Rare-gas Complexes, Clusters and Matrices. *Int. Rev. Phys. Chem.* **1999**, *18*, 485−556.
(9) Rojas-Lorenzo, G.; Rubayo-Soneira, J.; Alberti, S. F.; Chergui, M. Nonadiabatic Dynamics of Excited Hg($^3P_1$) in Ar Matrixes. *J. Phys. Chem. A* **2003**, *107*, 8225−8231.
(10) Rojas-Lorenzo, G.; Rubayo-Soneira, J.; Alberti, S. F. Dynamics of Exciplex Formation in Rare Gas Media. *Chem. Phys.* **2009**, *362*, 34−40.
(11) Collier, M. A.; McCaffrey, J. G. A Pair-potentials Analysis of the Emission Spectroscopy of $^3P_1$ State Atomic Mercury Isolated in Solid Ar, Kr, and Xe. *J. Chem. Phys.* **2003**, *119*, 11888−11898.
(12) Zuniga, J.; Bastida, A.; Requena, A.; Halberstadt, N.; Beswick, J. A. A Theoretical-Study of the $HgAr_2$($^3P_1$-$^1S_0$) Vibronic Spectrum. *J. Chem. Phys.* **1993**, *98*, 1007−1017.
(13) Okunishi, M.; Nakazawa, H.; Yamanouchi, K.; Tsuchiya, S. Interatomic Potentials of HgKr and HgXe Van der waals Complexes in the A^30^+ and B^31 States: Revisited. *J. Chem. Phys.* **1990**, *93*, 7526−7527.
(14) Ashcroft, N. W.; Mermin, N. D. *Solid State Physics*. Holt: New York, 1976.
(15) Klein, M. L.; Venables, J. A. *Rare Gas Solids*. Academic Press,: London, New York, 1977.
(16) Bastida, A.; Zuniga, J.; Requena, A.; Halberstadt, N.; Beswick, J. A. Excited-State Dynamics in $HgAr_2$ - Statistical-Analysis of Vibrational-State Distribution. *Faraday Discuss.* **1994**, *97*, 131−142.
(17) Tully, J. C. Mixed Quantum-Classical Dynamics. *Faraday Discuss.* **1998**, *110*, 407−419.
(18) Kohen, D.; Stillinger, F. H.; Tully, J. C. Model Studies of Nonadiabatic Dynamics. *J. Chem. Phys.* **1998**, *109*, 4713−4725.
(19) Bergsma, J. P.; Berens, P. H.; Wilson, K. R.; Fredkin, D. R.; Heller, E. J. Electronic-Spectra from Molecular-Dynamics: A Simple Approach. *J. Phys. Chem.* **1984**, *88*, 612−619.
(20) Berendsen, H. J. C.; Postma, J. P. M.; Vangunsteren, W. F.; Dinola, A.; Haak, J. R. Molecular-Dynamics with Coupling to an External Bath. *J. Chem. Phys.* **1984**, *81*, 3684−3690.
(21) Kramida, A. E. Atomic Spectra Database (version 5.1) (accessed June 13, 2014).
(22) Ryan, M.; Collier, M.; de Pujo, P.; Crépin, C.; McCaffrey, J. G. Investigations of the Optical Spectroscopy of Atomic Sodium Isolated in Solid Argon and Krypton: Experiments and Simulations. *J. Phys. Chem. A* **2010**, *114*, 3011−3024.
(23) Jacquet, E.; Zanuttini, D.; Douady, J.; Giglio, E.; Gervais, B. Spectroscopic Properties of Alkali Atoms Embedded in Ar Matrix. *J. Chem. Phys.* **2011**, *135*, 174503.